AIAA JOURNAL
Vol. 47, No. 7, July 2009

Prediction of Distortion of Airframe Components Made from Aluminum Plates

Sebastian Nervi*
Engineering Software Research and Development, Inc., Saint Louis, Missouri 63146
Barna A. Szabó†
Washington University in Saint Louis, Saint Louis, Missouri 63130
and
Keith A. Young‡
The Boeing Company, Saint Louis, Missouri 63166

DOI: 10.2514/1.37233

A mathematical model formulated for the prediction of distortion of airframe components manufactured from 7050-T7451 aluminum plates, caused by residual stresses introduced by the manufacturing process of the plate, was tested in validation experiments. The results indicate that distortion in thin gauge parts is caused primarily by machining-induced residual stresses. The residual stresses introduced by the plate manufacturing process, which includes hot rolling, quenching stretching, and aging operations, have a minor effect on distortion, consistent with the predictions based on the mathematical model described herein.

Nomenclature

A_{1j}	=	coefficients in the series expansion for the strains in direction 1
A_{2j}	=	coefficients in the series expansion for the strains in direction 2
a_k	=	depth of slot k, mm
$B(u_i, v_i)$	=	virtual work
E	=	modulus of elasticity, GPa
$E(\Omega)$	=	energy space
$e_{\max}$	=	relative error in maximum norm
G	=	Lamè constant, Gpa
h	=	plate thickness, mm
K	=	total number of slot increments
M	=	total number of strain gauges
N_1	=	number of terms in the series expansion for the strains in direction 1
N_2	=	number of terms in the series expansion for the strains in direction 2
n_i	=	unit normal to the boundary $\partial\Omega$
P_i	=	Legendre polynomial of degree i
$r_k^{(m)}$	=	strain reading in gauge location m corresponding to a_k
S_{ij}^k	=	stress field after cut k
T_i	=	tractions specified on the boundary $\partial\Omega$
t_i	=	nominal thickness of test article i, mm
t_{pl}	=	thickness of the surface layer, mm
U_i, u_i, v_i	=	displacement fields in $\mathbb{R}^3$
X_i	=	local coordinates of the plate
x, y, z	=	local coordinates of the test articles
x_i	=	local coordinates of the samples
α_{ij}	=	tensor of coefficients of thermal expansion, $1/°C$
Γ_i	=	cutting path i
$\Delta\mathcal{T}$	=	constant temperature change, °C
$\partial\Omega_i$	=	boundary of the elastic body i
ε_{ij}	=	strain tensor
$\varepsilon_{1kj}^{(m)}$	=	computed strain in gauge location m for a given a_k and P_j (direction 1)
$\varepsilon_{2kj}^{(m)}$	=	computed strain in gauge location m for a given a_k and P_j (direction 2)
η	=	dimensionless variable, $\eta = 2x_3/h$
λ	=	Lamè constant, GPa
ν	=	Poisson's ratio
ρ	=	density, kg/mm^3
σ_{ij}^0	=	residual stress tensor in Ω_0
$\sigma_1^{(R)}$	=	residual stress in direction 1
$\sigma_2^{(R)}$	=	residual stress in direction 2
Ω_i	=	domain of the elastic body i

Received 20 February 2008; revision received 23 December 2008; accepted for publication 5 March 2009.

*Research Scientist, Research and Development Group, 111 West Port Plaza, Suite 825. Member AIAA.

†Senior Professor, Department of Mechanical, Aerospace and Structural Engineering, One Brookings Drive, Campus Box 1185.

‡Research Engineer, Boeing's Advanced Manufacturing Research and Development Group in Saint Louis.

I. Introduction

INCREASED emphasis on affordability has led to a number of advances in airframe design and production. In an effort to reduce part count and assembly times, built-up components made from sheet metal are being replaced by unitized airframe components. Examples are complete wing skeletons, bulkheads, and control surfaces. The development of high-speed machining (HSM) techniques has enabled the economical fabrication of thin, lightweight structural components to provide improved performance. However, thin, unitized structural components manufactured by HSM techniques tend to exhibit substantial amounts of distortion caused by residual stresses.

Part distortion hinders the full implementation of new technologies and achievement of the significant cost savings they offer. The complex component configurations resulting from structural unification, with wide variations in geometry, increase the likelihood for excessive distortion. Manufacturing techniques that will enable the production of airframe components to tight tolerances need to be developed.

Distortion of airframe components is caused by two kinds of residual stresses: bulk stresses and machining-induced stresses. Bulk stresses are caused by the manufacturing process of the plates. The machining-induced residual stresses typically have high values within a very thin layer (0.1–0.5 mm) at the machined surface and decay rapidly with distance from the surface. The effect of

machining-induced residual stress on distortion tends to increase with decreasing thickness.

Our specific objectives of the investigations described herein were to formulate and test a mathematical model for the prediction of distortion of airframe components caused by bulk stresses. The scope of the present investigation is restricted to hot rolled aluminum plates; the specific focus is on 7050-T7451 aluminum plates, typically ranging in thickness from 6.35 to 152.4 mm.

The formulation and testing of mathematical models involve the following steps:

1) A mathematical problem is formulated, virtual experimentation is performed, and the parameters that characterize the initial conditions, material properties, and the boundary conditions are determined.

a) Conceptual development: A statement of the intended use of the model and identification of the key factors that are expected to have significant influence on predictions based on the mathematical model.

b) Calibration: Determination of the data required by the mathematical model, such as material properties and the initial stress distribution in the plate. In the interpretation of calibration experiments, the mathematical model is assumed to be correct.

c) Virtual experimentation: Using the mathematical model, studies are performed with the objective of testing the sensitivity of the data of interest to various modeling assumptions.

d) Design of validation experiments: The purpose of validation experiments is to test the predictive capabilities of the mathematical model. Metrics are defined and criteria are formulated that depend on the purpose of computation. Based on the metrics and criteria, the results of the validation experiments are evaluated. See, for example, [1].

2) The solution of the mathematical problem is approximated by numerical means and the data of interest are verified to be within acceptable tolerances.

3) Validation experiments are performed and the results of the validation experiments are evaluated. If the predictions do not exceed the stated criteria, then the model is said to have passed the validation test; otherwise, the causes of the difference between the prediction and experimental observation must be investigated and a new mathematical model formulated. In this case, the validation experiment is reclassified as a calibration experiment and a new validation experiment must be designed and executed.

For further information on validation, we refer to a guide issued by the American Society of Mechanical Engineers [2] in 2006. Because uncertainties are present in the geometrical description, material properties loading, and constraints, any comparison between the predicted and measured data involves statistical considerations [3,4].

When comparing experimental data with predictions based on a mathematical model, one must account for 1) errors in the mathematical model itself, including the conceptual formulation of the model, systematic and random errors in dimensions, material properties, and boundary conditions; 2) systematic and random errors in the experimental observations; and 3) errors in the numerical approximation of the solution of the mathematical model. To test a mathematical model, it is necessary to control both the experimental errors and the errors of discretization to within small tolerances.

II. Mathematical Model

We denote the material points of an elastic body by $\Omega_0 \subset \mathbb{R}^3$ and its boundary by $\partial\Omega_0$. The unit normal to the boundary is denoted by n_i^0. The residual stresses, denoted by σ_{ij}^0, must satisfy the equations of equilibrium and the stress-free boundary conditions. Assuming that the body is not constrained,

$$\sigma_{ij,j}^0 = 0 \quad \text{on } \Omega_0, \qquad \sigma_{ij}^0 n_j^0 = 0 \quad \text{on } \partial\Omega_0 \tag{1}$$

The mathematical model is based on the following assumptions: 1) the material is linearly elastic and remains linearly elastic throughout the machining process, 2) residual stresses introduced by the machining process can be neglected, 3) the elastic properties are known in every point in Ω_0, 4) the residual stresses are known functions of the spatial coordinates, and 5) the grips used for constraining the workpiece do not introduce stresses that would significantly affect the measurements of strains caused by the residual stresses. Assumptions 1 and 2 imply that the principle of superposition is applicable throughout the machining process in which the workpiece is systematically altered, that is, $\Omega_0 \to \Omega_1 \to \Omega_2 \cdots$ (where $\Omega_{i+1} \subset \Omega_i$); hence, the following theorem holds:

Theorem 1: In any given configuration of the elastic body, the residual stress distribution depends on σ_{ij}^0 defined on Ω_0 and the current configuration Ω_k $(k = 1, 2, \ldots, n)$, but not on the intervening configurations.

Proof: The residual stress satisfies Eq. (1). Let us now introduce a cut Γ_1 that produces the domain Ω_1 and a second cut Γ_2 that produces domain Ω_2. Denote the displacement field following the first (respectively, the second) cut by U_i^1 (respectively, U_i^2). The notation is shown in Fig. 1.

By the principle of superposition, U_i^1 satisfies

$$B(U_i^1, v_i) = -\int_{\Gamma_1} \sigma_{ij}^0 n_j v_i \, \mathrm{d}S \quad \forall\, v_i \in E(\Omega_1) \tag{2}$$

where $B(U_i^1, v_i)$ is the virtual work of internal stresses corresponding to the virtual displacement v_i on Ω_1. $E(\Omega_1)$ is the energy space defined by

$$E(\Omega_1) = \{B(u_i, u_i) \le C < \infty\}$$

Denote the stress field corresponding to U_i^1 on Ω_1 by S_{ij}^1, and let u_i^2 be the displacement field on Ω_2 corresponding to the tractions $S_{ij}^1 n_j$ acting on Γ_2. Therefore,

$$B(u_i^2, v_i) = \int_{\Gamma_2} S_{ij}^1 n_j v_i \, \mathrm{d}S \quad \forall\, v_i \in E(\Omega_2) \tag{3}$$

The displacement field corresponding to the second cut is $U_i^2 = u_i^2 + \tilde{U}_i^2$, where

$$B(\tilde{U}_i^2, v_i) = -\int_{\Gamma_2} (\sigma_{ij}^0 + S_{ij}^1) n_j v_i \, \mathrm{d}S \quad \forall\, v_i \in E(\Omega_2) \tag{4}$$

Adding Eqs. (3) and (4), we find that

$$B(U_i^2, v_i) = -\int_{\Gamma_2} \sigma_{ij}^0 n_j v_i \, \mathrm{d}S \quad \forall\, v_i \in E(\Omega_2) \tag{5}$$

which completes the proof. □

Using this theorem, the mathematical model is formulated as follows. Given the residual stress distribution σ_{ij}^0 on an initial configuration Ω_0, solve the Navier–Lamè equations on any configuration $\Omega \subset \Omega_0$, with the tractions $T_i = -\sigma_{ij}^0 n_j$ specified on the boundary $\partial\Omega$. Formally,

$$G u_{i,jj} + (\lambda + G) u_{j,ji} = 0 \quad \text{on } \Omega, \qquad T_i = -\sigma_{ij}^0 n_j \quad \text{on } \partial\Omega \tag{6}$$

This problem cast in the generalized form is

$$\int_\Omega (\lambda \epsilon_{kk}^{(u)} \epsilon_{ii}^{(v)} + 2G \epsilon_{ij}^{(u)} \epsilon_{ij}^{(v)}) \, \mathrm{d}V = -\int_{\partial\Omega} \sigma_{ij}^0 n_j v_i \, \mathrm{d}S \tag{7}$$

where $\epsilon_{ij}^{(u)} = (u_{i,j} + u_{j,i})$ is the infinitesimal strain tensor and v_i is a test function. Equation (7) holds for all vector functions u_i and v_i for which the indicated operations are defined.

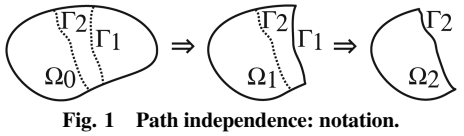

Fig. 1 Path independence: notation.

Because $\sigma^0_{ij,j} = 0$, on applying the divergence theorem to the right-hand side of Eq. (7) we have

$$\int_\Omega (\lambda \epsilon^{(u)}_{kk} \epsilon^{(v)}_{ii} + 2G\epsilon^{(u)}_{ij}\epsilon^{(v)}_{ij})\,\mathrm{d}V = -\int_\Omega \sigma^0_{ij}\epsilon^{(v)}_{ij}\,\mathrm{d}V \tag{8}$$

which is analogous to the stationary thermoelastic problem in the sense that if we let

$$\sigma^0_{ij} = -(\lambda \alpha_{kk}\delta_{ij} + 2G\alpha_{ij})\Delta\mathcal{T} \tag{9}$$

where α_{ij} is the tensor of coefficients of thermal expansion and $\Delta\mathcal{T}$ is a constant temperature change, then Eq. (8) becomes a problem of thermoelasticity with zero initial stresses.

In view of Theorem 1, the displacement field U^k_i and the corresponding stress field defined S^k_{ij}, defined on Ω_k, are linear functions of σ^0_{ij} defined on Ω_0.

III. Calibration

The purpose of calibration experiments is to determine physical properties and other model parameters through experimental observations. Here we focus on 1) estimation of bulk stresses in a 7050-T7451 aluminum plate, and 2) estimation of the thickness of the surface layer where machining-induced residual stresses dominate.

The material properties used in the model were nominal values for 7050-T7451 aluminum plates: modulus of elasticity $E=$ 70.07 GPa, Poisson's ratio $\nu = 0.33$, yield strength $\sigma_{\text{yield}}=$ 490 MPa, and density $\rho = 2.874 \times 10^{-6}$ kg/mm^3.

Note that U.S. customary units were used in the original work [5,6].

A. Estimation of the Bulk Stress

We estimate the bulk stress σ^0_{ij} by 1) making certain assumptions concerning its distribution in the plate; 2) removing samples from the plate; 3) progressively changing the configuration Ω_k, $k = 0, 1, 2, \ldots, K$ of each sample, that is, $\Omega_{k+1} \subset \Omega_k$; and 4) measuring the strains corresponding to the stress field S^k_{ij}, which, in accordance with Theorem 1, is a function of Ω_k and σ^0_{ij} only. From the measured strains and the assumed distribution of σ^0_{ij}, an estimate of σ^0_{ij} is obtained.

Six samples, measuring $98.425 \times 101.6 \times 304.8$ mm were removed from a 101.6-mm-thick plate by saw cut. The other dimensions of the plate are shown in Fig. 2.

Three of the samples were oriented such that the long axis was in the rolling direction; the other three were oriented with the long axis in the transverse direction. The location and numbering of the samples is shown in Fig. 2. By convention, the rolling direction is labeled L (longitudinal), the transverse direction is labeled LT (long transverse), and the thickness direction is labeled ST (short transverse). The coordinate axis in the ST direction will be denoted as x_3 for the samples.

Ideally, the location of the samples would be sufficiently far from the boundaries of the plate to justify the assumption that the residual stresses are functions of the x_3 coordinate only. This condition could not be fully satisfied; therefore, errors were introduced in the interpretation of the calibration experiments. These errors affect the predictions based on computed information. This point will be discussed in Sec. VI.F.

In the following text, we will use the notation (X_1, X_2, X_3) to identify the local coordinates for the plate, (x_1, x_2, x_3) for the samples, and (x, y, z) for the test articles. Note that $X_3 \equiv x_3 \equiv z$.

Six strain gauges (Micro-Measurements CEA-13-250UW-350) were attached to each of the samples. The location of the strain gauges are shown in Fig. 3a. The samples were clamped such that they acted like cantilever beams. The clamped surfaces are indicated in Fig. 3a by the shaded region.

Slots were machined using a 19.05-mm-diam milling tool with a 3.048 mm corner radius and two flutes. The depth of the slot a_k, defined in Fig. 3a, was progressively increased and, for each value of

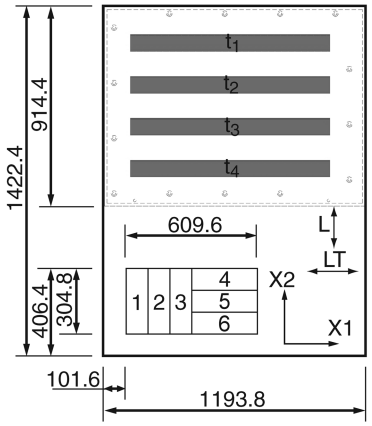

a)

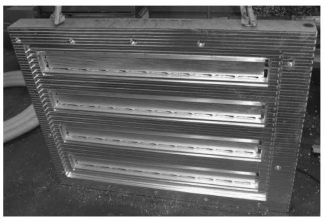

b)

Fig. 2 Shown are the following: a) location and numbering of the samples and the test articles (dimensions are in millimeters), and b) test articles after machining.

a_k $(k = 0, 1, 2, \ldots, K,$ where $a_0 = 0)$, the strain readings were recorded. The strain reading in gauge location m corresponding to a_k is denoted as $r^{(m)}_k$ $(m = 1, 2, \ldots, M,\ k = 0, 1, 2, \ldots, K)$, where $r^{(m)}_0 = 0$. In this investigation, $M = 6$ and $K = 43$ were used. The strain gauges installed on the side surfaces were sacrificed in the course of the machining process, as shown in Fig. 3b.

We introduce the dimensionless variable $\eta = 2x_3/h$, $-h/2 \le x_3 \le h/2$ and denote the Legendre polynomial of degree i as $P_i(\eta)$.

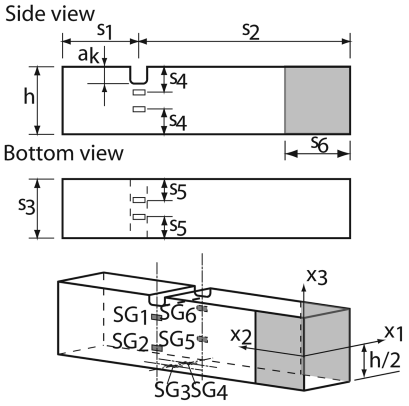

a)

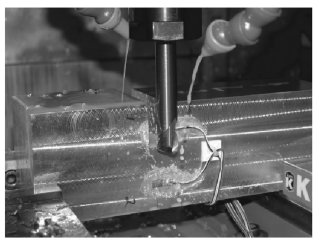

b)

Fig. 3 Strain gauge locations and dimensions of bar specimens (dimensions are in millimeters): $s_1 = 101.6$, $s_2 = 203.2$, $s_3 = 98.435$, $s_1 = 25.4$, $s_5 = 38.1$, $s_6 = 57.15$, and $h = 101.6$.

Referring to Eq. (9), for each value of a_k, we let $(\alpha_1 \Delta\mathcal{T})_j = P_{j+1}(\eta)$, $j = 1, 2, \ldots, N_1$ and compute the strain component corresponding to the strain measured in gauge location m. We denote the computed strain values as $\epsilon_{1kj}^{(m)}$. Similarly, we let $(\alpha_2 \Delta\mathcal{T})_j = P_{j+1}(\eta)$, $j = 1, 2, \ldots, N_2$ and compute the strain in gauge location m for each a_k. We denote the computed strain values as $\epsilon_{2kj}^{(m)}$. The strain $\epsilon_{1kj}^{(m)}$ (respectively, $\epsilon_{2kj}^{(m)}$) is the influence coefficient corresponding to $\sigma_{11}^0 = P_{j+1}(\eta)$ (respectively, $\sigma_{22}^0 = P_{j+1}(\eta)$) on the domain Ω_k.

The computations were performed in three dimensions. Interpretation of the experimental information by means of three-dimensional analysis permits one to make independent assumptions about the distribution of residual stresses in the rolling and transverse directions. Additional considerations concerning the interpretation of experimental data were presented by Nervi and Szabó [7].

Using the principle of superposition,

$$r_k^{(m)} \approx \sum_{j=1}^{N_1} A_{1j}(\epsilon_{1kj}^{(m)} - \epsilon_{10j}^{(m)}) + \sum_{j=1}^{N_2} A_{2j}(\epsilon_{2kj}^{(m)} - \epsilon_{20j}^{(m)}) \qquad (10)$$

Note that the strain readings are with reference to the sample before making the first cut ($k = 0$); therefore, the influence coefficients are $\epsilon_{1kj}^{(m)} - \epsilon_{10j}^{(m)}$ and $\epsilon_{2kj}^{(m)} - \epsilon_{20j}^{(m)}$.

From these equations, the coefficients A_{1j} and A_{2j} were computed by least-squares fitting. In view of Eq. (9), the estimated residual stresses in the plate are

$$\sigma_1^{(R)} = -\frac{E\Delta\mathcal{T}}{1-\nu^2}\left(\sum_{j=1}^{N_1} A_{1j}P_{j+1}(\eta) + \nu\sum_{j=1}^{N_2} A_{2j}P_{j+1}(\eta)\right) \qquad (11)$$

$$\sigma_2^{(R)} = -\frac{E\Delta\mathcal{T}}{1-\nu^2}\left(\nu\sum_{j=1}^{N_1} A_{1j}P_{j+1}(\eta) + \sum_{j=1}^{N_2} A_{2j}P_{j+1}(\eta)\right) \qquad (12)$$

Because the residual stresses are assumed to be functions of x_3 only, the readings obtained from symmetrically located strain gauges should be the same up to experimental errors. Therefore, the average of symmetrically located strain gauges were used in the computation of the coefficients (A_{1j}, A_{2j}). Only half of the domain with symmetry conditions was used in the interpretation of the calibration experiments.

It is necessary to have a substantially larger number of observations than $N1 + N2$, that is, $(N1 + N2) \ll KM$. In this investigation, $N_1 = N_2 = 13$ (polynomial degree 14) was used. As K increases, the difference between consecutive strain readings (i.e., $\Delta r_k^{(m)} = r_k^{(m)} - r_{k-1}^{(m)}$) decreases. Therefore, it is not useful to have K larger than the value at which $\Delta r_k^{(m)}$ is comparable to the size of the errors in the strain measurement. Not all observations are equally reliable because it is not possible to measure small strains accurately. The strain gauges were oriented so as to maximize the strain readings.

The estimated residual stress distributions for the rolling and transverse directions are shown in Figs. 4 and 5. The stress distribution and magnitude are similar to results obtained by other investigators [8]. The bounds, indicated as "max" and "min," are computed using the maximum and minimum values of the measured strains.

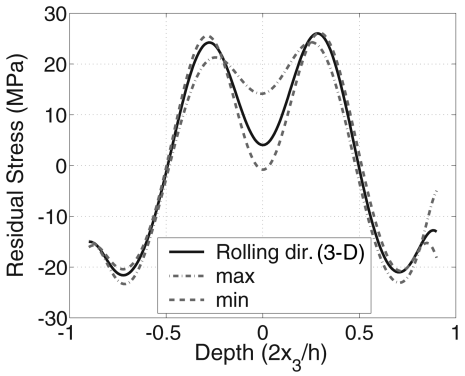

Fig. 4 Residual stress distribution in the rolling direction.

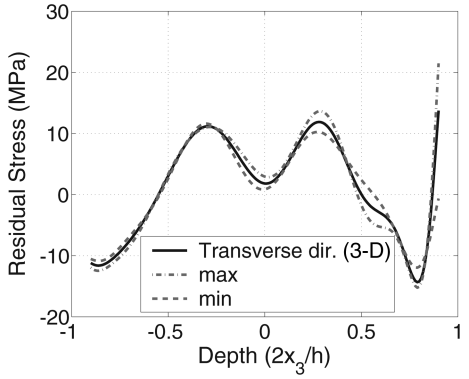

Fig. 5 Residual stress distribution in the transverse direction.

By numerical experimentation it was found that the results shown in Figs. 4 and 5 changed by a negligible amount in the range of $|\eta| \leq 0.9$ for $(N_1, N_2) \geq 11$. The stresses near the surfaces ($0.9 < |\eta| \leq 1$) are not reported because the signal-to-noise ratio is small in those regions; therefore, the measurements are unreliable.

B. Estimation of the Thickness of the Surface Layer

The mathematical model considered herein does not account for machining-induced residual stresses. Therefore, predictions of distortion will be reliable only if the machining-induced residual stresses can be neglected. Determination of the distribution of machining-induced residual stresses is a difficult problem. In the present investigation, we focused on estimating the average thickness of the surface layer where machining-induced residual stresses dominate. This layer is caused by the large plastic strain imposed by the cutting tool. The estimation is based on the assumption that the average residual stresses caused by machining decay exponentially with distance from the surface, as indicated schematically in Fig. 6.

Experiments were performed to estimate the thickness of the surface layer, t_{pl}. In these experiments, small plates were machined with the head of the tool (web specimens) and the side of the tool (rib specimens). The surface layer of each specimen was removed by chemical milling, and the resulting change in configuration was measured. The details of these experiments and their interpretation are described in [5,6,9].

Based on the results of these experiments, the thickness of the surface layer was estimated to be less than 0.25 mm.

IV. Virtual Experimentation

Virtual experimentation is useful for testing assumptions incorporated in the mathematical model. The effects of the constraint conditions and gravity were investigated.

A. Effect of Constraints

To study the effect of the constraints, the strains at the strain gauge locations, corresponding to various clamping conditions, were computed. It was found that the effect of alternative clamping conditions was smaller than the strain gauge error ($\pm 2\mu$).

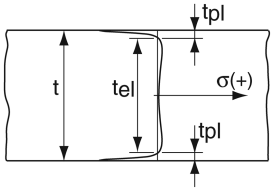

Fig. 6 Schematic representation of the residual stresses caused by machining.

B. Effects of Gravity

Because the specimens are of substantial size, the effects of gravity on the strain gauge readings were simulated in numerical experiments. It was found that the effects of gravity are negligible.

The spatial configuration of the test articles was measured while they were supported in three points using an adhesive to keep them in place. The effect of gravity on the configuration of the test articles was simulated in virtual experiments and was found to be less than the measurement error.

V. Verification

Verification is a process by which it is ascertained that the computed data are within acceptable tolerances. In this investigation, all computations and verification procedures were performed with StressCheck® [10]. The errors of approximation were controlled by means of p-extension [11]. For all solutions, the estimated relative error in energy norm was under 2%. For details, we refer to [10]. The convergence of the data of interest was monitored to ensure that the reported data are virtually independent of the discretization.

VI. Validation

The data obtained from the calibration experiments were incorporated in the mathematical model, which was then used for predicting the outcome of experiments specifically conceived and designed for validation.

The design of a validation experiment, which includes the establishment of metrics and criteria, depends on the intended use of the model. In this case, the intended use of the model was to predict whether the distortion of an airframe component, milled from a 7050-T7451 aluminum plate, would or would not be within allowed manufacturing tolerances.

A. Metrics and Criteria

In this investigation, the metric is the maximum difference between the corresponding surface points of the manufactured workpiece and its blueprint representation when the workpiece is positioned so as to minimize the rms measure of the distances between the corresponding points.

The criteria are based on manufacturing tolerances established by various conventions and specifications. The following tolerances are considered to be typical for airframe manufacturers: ± 0.25 mm for thickness, ± 0.25 mm for all mold line or mating surfaces, ± 0.50 mm for profile tolerance, and ± 0.75 mm for all nonmating rib and flange locations.

Parts exceeding these tolerances are acceptable, provided that the following conditions are met:

1) All flat parts less than 4.06 mm thick shall be capable of being brought to within blueprint tolerances by the application of light pressure, the resultant of which must not exceed 44.5 N. The light pressure is allowed to be applied anywhere on the part in the course of inspection.

2) All parts thicker than 4.06 mm and those which are integrally stiffened shall be capable of being brought to within blueprint tolerances by the application of light pressure, the resultant of which must not exceed 222 N. The light pressure is allowed to be applied anywhere on the part in the course of inspection.

3) If an aluminum part is buckled following machining operations, then it is rejected. Reworking such parts is not allowed.

This information was collected through interviews with engineers who have extensive experience in this area. The criterion was that the model would be rejected if it failed to predict whether the test articles would or would not be within the manufacturing tolerances.

B. Test Articles

Four test articles were machined from a 101.6-mm-thick 7050-T7451 aluminum plate. The cross sections were Z shaped and of constant thickness. The dimensions are shown in Fig. 7. The nominal thicknesses were $t_1 = 3.302$, $t_2 = 2.286$, $t_3 = 1.778$, and $t_4 = 1.270$ mm. The thicknesses of the test articles were chosen so that $t_{i+1} \geq t_i + 2t_{\text{pl}}$ $(i = 1, 2, 3)$, where t_{pl} is the maximum estimated thickness of the machining-induced surface layer.

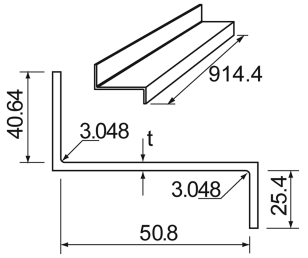

Fig. 7 Dimensions of the test articles in millimeters.

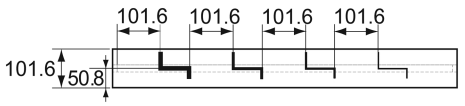

Fig. 8 Location of the test articles with respect to the plate (dimensions are in millimeters).

The test articles were roughed with a 19.05-mm-diam tool with a 3.048 mm corner radius to within 5.08 mm of the finished part then, finished with a 12.7-mm-diam, 35 deg helix, 3.048 mm corner radius tool with a 0.127 mm radius of wear. The ribs of the test articles were machined with the side of the tool, and the web was machined with the end of the tool.

During finishing, the axial depth of the cut was 1.27 mm and the radial depth was 5.08 mm. The tool was operated at 32,000 rpm and a 135 mm/s feed rate. The location of the test articles with respect to the plate is shown in Figs. 2 and 8.

C. Validation Protocol

The experiments were designed to meet the criteria for validation experiments [1,12]. The numerical simulations were performed independently and before the experiments. Only after all experiments and numerical simulations were completed were the results compared. In other words, the prediction was "blind."

The following information was available for the prediction: 1) the bulk stresses (obtained experimentally from samples taken from the same plate stock from which the test articles were machined), 2) the through thickness location of the specimens in the plate, 3) the ideal (blueprint) geometry of the specimens, and 4) the average thickness of the flanges and web as manufactured.

The shape and dimensions of the test articles were designed by the analyst and the experimentalist so that the test articles were representative of airframe components, but simple enough to facilitate the experimental measurements.

Table 1 Thicknesses of the test articles after machining

Specimen, mm	Max.	Min.	Av.
		Rib_1	
t_1	3.2436	3.2258	3.2329
t_2	2.2301	2.2073	2.2162
t_3	1.7120	1.6942	1.7011
t_4	1.2141	1.1887	1.1969
		Web	
t_1	3.2131	3.0455	3.1437
t_2	2.2581	2.0396	2.1668
t_3	1.7755	1.5697	1.6822
t_4	1.2827	1.0795	1.1886
		Rib_2	
t_1	3.2487	3.2283	3.2378
t_2	2.2301	2.2123	2.2197
t_3	1.7170	1.7018	1.7088
t_4	1.2040	1.1786	1.1938

D. Measurements

After machining, the test articles were measured to check for thickness variations. The thicknesses were found to be smaller than the design value; the maximum measured thickness difference was approximately 0.254 mm. The measured thickness of each test article is given in Table 1. The definition of Rib_1, Rib_2, and Web is given in Fig. 9. The numerical analysis was based on the average thicknesses.

The spatial configuration of the test articles was measured with a Delta DEA model 340 coordinate measuring machine (CMM) using a Renishaw contact probe. The accuracy of this CMM over a volume of $3.0 \times 1.5 \times 1.0$ m^3 is 0.056 mm. The repeatability of the probe is certified to be within 0.028 mm. The location and numbering of the measured points are shown in Fig. 9.

The experimental data were linearly transformed so that both the experimental and analytical data were in the same reference frame.

E. Comparison of Predicted and Observed Configurations

The predicted and measured configurations of the test articles following machining are shown on a typical cross section in Fig. 10. The reference (heavy dashed line) represents the location of the blueprint surface and corresponds to the solid lines in Fig. 9; the tolerances (light solid line and light dashed line) represent the range of acceptable tolerance for distortion.

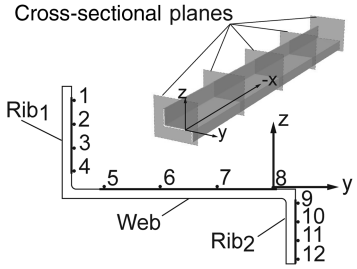

Fig. 9 Cross-sectional planes: location and numbering of measured points.

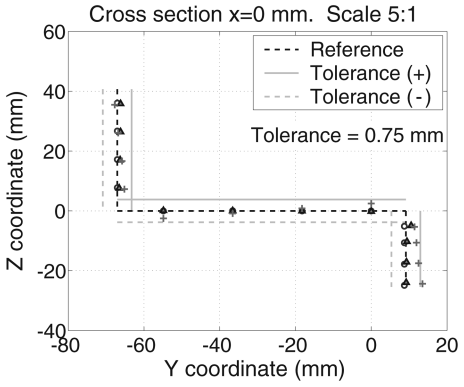

Fig. 10 Configuration after machining (cross), after chemical milling (triangle), and prediction (circle) for the t_2 specimen.

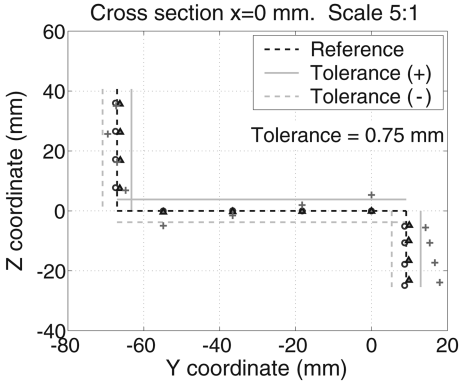

Fig. 11 Configuration after machining (cross), after chemical milling (triangle), and prediction (circle) for the t_4 specimen.

Table 2 Specimen thicknesses after layer removal by chemical milling

Specimen, mm	Max.	Min.	Av.
		Rib_1	
t_2	2.1082	2.0574	2.0828
t_4	1.0668	1.016	1.0414
		Web	
t_2	2.159	2.0066	2.0828
t_4	1.143	1.1176	1.1303
		Rib_2	
t_2	2.0574	2.032	2.0447
t_4	1.016	1.016	1.016

It is seen that the predicted and observed configurations differ substantially. Furthermore, the predicted dominant deformation was bowing about the local y axis (the L direction), whereas the observed dominant configuration was twisting about the local x axis (the LT direction). It should be recalled, however, that the mathematical model does not account for residual stresses induced by machining; therefore, the data shown in Figs. 10 and 11 for two different thicknesses cannot be compared with the predicted data.

It was also observed that the distortion was similar (i.e., dominant twisting about the local x axis) for all test articles and increased with decreasing thickness of the test articles. This is consistent with the assumption that the machining-induced surface layer is removed and recreated at each pass of the cutting tool. Therefore, the machining-induced residual stresses depend only on the parameters of the cutting process and the material, provided that there is an elastic core of sufficient size to equilibrate the machining-induced stresses.

Following measurement of the test articles after machining, the specimens $t_1^{(\text{avg})} = 3.205$ and $t_2^{(\text{avg})} = 2.019$ mm were chemically milled to remove a layer of material slightly larger than the thickness of the estimated plastic layer to a final thickness of approximately $t^{(\text{avg})} = 2.286$ and $t^{(\text{avg})} = 1.270$ mm, respectively. The thickness of the plastic layer was estimated to be $t_{\text{pl}} \leq 0.25$ mm; therefore, it is reasonable to assume that chemical milling removed the machining-induced stresses. After chemical milling, the thickness of each test article was measured. The measured values of thickness are given in Table 2.

The thickness of the chemically milled test article t_1 (respectively, t_2) was approximately equal to the thickness of the machined test article t_2 (respectively, t_4). This allowed the comparison of test articles of similar thickness for which the distortion was caused primarily by the machining-induced residual stress (t_2 and t_4) and by the bulk stresses (t_1 and t_2, following chemical milling).

The measured and predicted distortions of the specimens after chemical milling is shown for typical cross sections in Figs. 10 and 11 for two different thicknesses. It is seen that chemical milling significantly reduced the magnitude of distortion and that the predicted and measured distortions are very close. This indicates that the mathematical model successfully predicted the magnitude of the distortion caused by bulk stresses. However, the bulk stresses are not the primary cause of distortion for parts of small thickness; the machining-induced residual stresses are.

F. Sources of Error and Uncertainty

The following are considered to be the primary sources of error and uncertainty in order of importance:

1) *Errors in the estimated residual stresses*. Two of the key assumptions incorporated in the mathematical model are that the residual stresses are functions of x_3 only and that the principal axes are aligned with the rolling and transverse directions. These assumptions are justified when the plate is large but do not hold near the edge of the plate where the boundary-layer effects influence the distribution of residual stresses [7]. The calibration experiments performed as part of this investigation indicated variations as large as

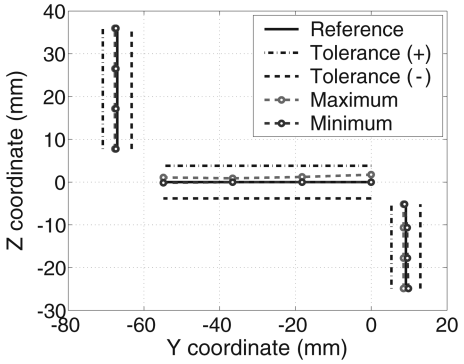

Fig. 12 Range of prediction for specimen of thickness t_2.

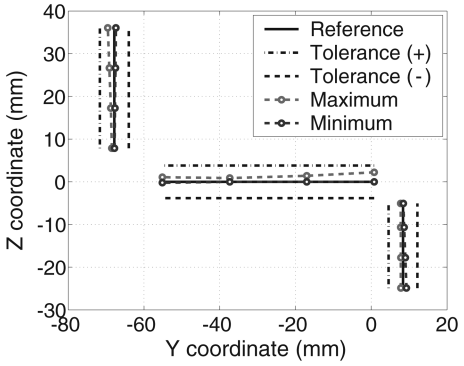

Fig. 13 Range of prediction for specimen of thickness t_4.

38.5% (respectively, 23.0%) in the residual stress profile in the rolling (respectively, transverse) direction measured in the maximum norm defined as:

$$e_{\max} = 100\frac{\max(|\sigma_{\max} - \sigma_{\text{ave}}|, |\sigma_{\min} - \sigma_{\text{ave}}|)}{\max|\sigma_{\text{ave}}|}$$

where $\sigma_{\max}$, $\sigma_{\min}$, and σ_{ave} are shown in Figs. 4 and 5 for the rolling and transverse directions, respectively.

Figures 12 and 13 show the maximum and minimum predicted distortion at the measurement points for all cross sections computed for all the combinations of bulk stresses shown in Figs. 4 and 5. We observe that, for any given combination of bulk residual stresses, the predicted distortion will fall within the acceptable tolerance bounds and that the measured distortion for the chemically milled specimens fall within the range of predicted values.

2) *Variation in material properties*. The material properties used in the model were nominal values for 7050-T7451 aluminum plates; the specific elastic properties were not measured for the plate from which the test articles were machined and it was assumed that the material properties are constant over the plate.

3) *Variation in thickness*. In the numerical simulations, uniform thicknesses (the average thicknesses of the flanges and web as manufactured) were used. In reality, there were variations in thickness, as indicated in Tables 1 and 2. However, the maximum displacement changes only 16% for a 60% change in the average thickness; therefore, variations in thickness are not expected to generate significant variations in the predicted distortion.

4) *Errors in measurements*. The strain gauges used in the calibration and the coordinate measuring machine impose certain limitations on the accuracy of observation.

VII. Conclusions

The following conclusions can be drawn from the present investigation.

1) The mathematical model passed the validation test that is, based on the metrics and criteria established for validation, no reason was found that would justify rejection of the model.

2) The magnitude of distortion of thin-walled test articles, typical of unitized airframe components made of 7050-T7451 aluminum plates, that can be attributed to the residual stresses caused by the plate manufacturing process is not substantial.

3) The primary cause of distortion is the presence of large residual stresses introduced into a thin surface layer by machining. Therefore, the minimization of machining-induced residual stresses or the removal of the surface layer by mechanical or chemical means will significantly reduce distortion.

4) The accuracy of predictions based on any mathematical model is, of course, influenced by uncertainties in the input data. The largest uncertainty is associated with the distribution of residual stresses in the plate. Because the number of specimens available for the calibration experiments was small, reliable quantification of uncertainty is not possible. We can offer only our subjective judgment in estimating that predictions of maximum distortion based on the procedures described herein will be within a 40% relative error.

Acknowledgments

The writers wish to thank Ivo Babuška for his constructive comments on the manuscript of this paper. This work was sponsored in part by the Air Force Office of Scientific Research, U.S. Air Force, under grant FA9550-05-1-0105. The views and conclusions contained herein are those of the authors and should not be interpreted as necessarily representing the official policies or endorsements, either expressed or implied, of the Air Force Office of Scientific Research or the U.S. Government.

References

[1] Oberkampf, W., "What Are Validation Experiments?" *Experimental Techniques*, Vol. 25, 2001, pp. 35–40. doi:10.1111/j.1747-1567.2001.tb00023.x

[2] "Guide for Verification and Validation in Computational Solid Mechanics," V&V 10-2006, *The American Society of Mechanical Engineers*, New York, 2006, ISBN: 079183042X.

[3] Hills, R. G., and Trucano, T. G., "Statistical Validation of Engineering and Scientific Models: Background," Sandia National Laboratories Rept. SAND99-1256, 1999.

[4] Babuska, I., Nobile, F., and Tempone, R., "Reliability of Computational Science," *Numerical Methods for Partial Differential Equations*, Vol. 23, No. 4, 2007, pp. 753–784. doi:10.1002/num.20263, ISSN .

[5] Nervi, S., "A Mathematical Model for the Estimation of the Effects of Residual Stresses in Aluminum Plates," Ph.D. Dissertation, Washington Univ. in Saint Louis, St. Louis, MO, 2005.

[6] Young, K. A., "Machining-Induced Residual Stress and Distortion of Thin Parts," Ph.D. Dissertation, Washington Univ. in Saint Louis, St. Louis, MO, 2005.

[7] Nervi, S., and Szabó, B., "On the Estimation of Residual Stresses by the Crack Compliance Method," *Computer Methods in Applied Mechanics and Engineering*, Vol. 196, 2007, pp. 3577–3584. doi:10.1016/j.cma.2006.10.037

[8] Prime, M. B., and Hill, M. R., "Residual Stress, Stress Relief, and Inhomogeneity in Aluminum Plate," *Scripta Materialia*, Vol. 46, No. 1, 2002, pp. 77–82. doi:10.1016/S1359-6462(01)01201-5

[9] Young, K., Nervi, S., and Szabó, B., "Machining-Induced Residual Stress and Distortion," *2005 Transactions Journal of Aerospace*, Society of Automotive Engineers, Warrendale, PA, 2005, pp. 1030–1038.

[10] StressCheck® Master Guide, Release 7, Engineering Software Research & Development, Inc., St. Louis, MO, Dec. 2004.

[11] Szabó, B., and Babuška, I., *Finite Element Analysis*, Wiley, New York, 1991.

[12] Oberkampf, W., DeLand, S., Rutherford, B. M., Diegert, K., and Alvin, K., "Error and Uncertainty in Modelling and Simulation," *Reliability Engineering & System Safety*, Vol. 75, 2002, pp. 333–357. doi:10.1016/S0951-8320(01)00120-X

K. Shivakumar
Associate Editor